Comparison between AlN and Al_2O_3 ceramics applied to barrier dielectric of plasma actuator*

Dong-Liang Bian(卞栋梁)[1], Yun Wu(吴云)[2,†], Min Jia(贾敏)[1], Chang-Bai Long(龙昌柏)[1], and Sheng-Bo Jiao(焦胜博)[1]

[1] *Air Force Engineering University, Xi'an* 710038, *China*
[2] *Xi'an Jiaotong University, Xi'an* 710049, *China*

(Received 24 February 2017; revised manuscript received 13 April 2017; published online 20 June 2017)

This paper reports the material characterization and performance evaluation of an AlN ceramic based dielectric barrier discharge (DBD) plasma actuator. A conventional Al_2O_3 ceramic is also investigated as a control. The plasma images, thermal characteristics and electrical properties of the two actuators are compared and studied. Then, with the same electrical operating parameters (12-kV applied voltage and 11-kHz power frequency), variations of the surface morphologies, consumed power and induced velocities are recorded and analyzed. The experimental results show that the AlN actuator can produce a more uniform discharge while the discharge of the Al_2O_3 actuator is easier to become filamentary. The later condition leads to higher power consumption and earlier failure due to electrode oxidation. In the plasma process, the power increment of the AlN actuator is higher than that of the Al_2O_3 actuator. The induced velocity is also influenced by this process. Prior to aging, the maximum induced velocity of the AlN actuator is 4.2 m/s, which is about 40% higher than that of the Al_2O_3 actuator. After 120-min plasma aging, the maximum velocity of the aged AlN actuator decreases by 27.8% while the Al_2O_3 actuator registers a decrease of 25%.

Keywords: plasma, DBD, flow control, discharge, ionic wind, Al_2O_3 ceramic, AlN ceramic

PACS: 47.85.L–, 52.25.Mq, 52.50.–b, 81.05.Je **DOI:** 10.1088/1674-1056/26/8/084703

1. Introduction

Surface dielectric barrier discharge (SDBD) has been investigated over the past decade in the field of plasma flow control.[1,2] These actuators usually consist of two flat electrodes mounted asymmetrically on either side of a dielectric barrier. When subjected to a high ac voltage applied across the exposed and encapsulated electrodes, the actuator produces an electrically-generated plasma on the surface, where charged species are propelled by the electric field lines colliding with the surrounding air. Comprehensive reviews of physics, experiments and applications of the plasma actuator have been published by Moreau,[3] Corke,[4] Benard and Moreau.[5]

In the past, many papers have studied the properties of various dielectric materials on the performance of DBD plasma actuator. Forte *et al.*[6] demonstrated that under the same consumed electric power, the induced velocity of a Polymethyl methacrylate (PMMA) plate was higher than that of a glass flat plate. Pons *et al.*[7] and Dong *et al.*[8] showed that a decrease of the dielectric thickness led to the increase of maximum induced velocity. However, as the dielectric thickness decreases, the electric discharge is more likely to become filamentary at low applied voltage. In this instance, the discharge filaments usually concentrate at several injection points on the edge of the exposed electrode, which may result in premature dielectric breakdown[6] and may also reduce the efficiency of the plasma actuator.[9] To ensure a more uniform discharge, Thomas *et al.*[10] and Abe *et al.*[11] found that a thicker layer of the dielectric resulted in lower dielectric coefficient and higher dielectric strength. Durscher *et al.*[12] demonstrated that surface temperature of the actuator played a crucial role in the transition from glow discharge to filamentary discharge and the saturation effect can be controlled by changing the local temperature of the dielectric. Furthermore, novel dielectric barrier material[13–15] or material modification[16–18] have also been studied to improve the performance of the DBD actuator. In the area of novel dielectrics, Park *et al.*[13] demonstrated a flexible DBD reactor, which was composed of copper electrodes and two dielectric layers including water and Teflon tubes. This device produced a stable plasma discharge over a long period of operation due to the cooling of the insulation surface. Durscher and Roy[14] evaluated the performances of two new materials (silica aerogels and ferroelectrics) with extreme permittivity as dielectrics of the actuators, they found that silica aerogels exhibited an order of magnitude in weight ratio of thrust to actuator higher than acrylics. Afterwards, Michael and David[15] used ferroelectric crystal with a large permittivity and small coercive field in an actuator. The applied voltage that was required to generate a discharge and was found to be reduced to < 600 V in air. Using titania (TiO_2) as a plasma catalyst, Fine and Brickner[16] found that the mea-

*Project supported by the National Natural Science Foundation of China (Grant Nos. 51522606, 91541120, 51502346, and No.51407194).
†Corresponding author. E-mail: wuyun1223@126.com
© 2017 Chinese Physical Society and IOP Publishing Ltd

sured thrust was increased by as much as 120% with respect to the catalyst-free actuator. Starikovskiy and Miles[17] combined SiO_2 with a dielectric material by using ion-implants and ohmic connections to build a dielectric multilayer barrier that allowed a partial depletion of the accumulated charges to partially deplete. Opaits *et al.*[18] proposed the use of a slightly conductive silicon coating to permit the accumulated charges to leave from the surface of the dielectric barrier.

Layers of Kapton tape, which was comprised of alternative layers of polyimide film and a silicone-based adhesive, are usually used as the dielectric of a plasma actuator.[19,20] Although this approach works, it presents issues relating to discrete thickness, handling difficulties, partial discharge between layers[21] and most significantly, material degradation.[22] Therefore, after long-time plasma process, the top layer of the polyimide film usually degrades then the underlying adhesive appears.[20] Compared with the widely used polymer dielectrics, ceramic offers the advantages of corrosion resistance, high and low temperature resistance, excellent dielectric properties and heat conduction, which make it a good dielectric barrier candidate for the future. For example, after discharge aging, Pons *et al.*[23] observed very few evidences of degradation on ceramic plates. However, the material properties and performance of the ceramic actuator in the plasma process are still unknown.

In this paper, two different ceramics based DBD plasma actuators are investigated. Firstly, before dielectric aging, plasma images, thermal characteristics and electrical properties of the AlN actuator and the Al_2O_3 actuator are compared and discussed. Afterwards, the evolutions of the surface morphologies, plasma images, power consumption are monitored and analyzed at various operating times. A Digital microscope imaging system is further used to characterize changes in the surface morphology. Then, the induced velocities of the actuators are measured using a Pitot tube before and after plasma discharge aging.

2. Actuator and experimental apparatus

2.1. Actuator construction

The dielectric barriers used in the plasma actuators are 0.5-mm-thick AlN ceramic and Al_2O_3 ceramic, which are obtained from Jia Rifeng Electronic Material Co., Ltd (Shenzhen, China). As illustrated in Fig. 1, the electrodes (oblique line area) are fabricated through a screen-printing process and the material is silver slurry. The thickness of the electrodes is 10 ± 0.5 μm. Figure 1(a) shows the geometry of the exposed electrode. The length and width of one part along the Z direction are 40 mm and 3 mm, respectively. Another part of the exposed electrode along the X direction is used to attach to the wire. Figure 1(b) shows the geometry of the encapsulated electrode, which is 25 mm in width and 30 mm in length. Both ends of it close to the side of the exposed electrode are accurately rounded to avoid high-tension point discharge. There is no gap between the edges of two electrodes. The grounded electrode and upstream direction of the exposed electrode are covered with Kapton tape to prevent unwanted plasma from forming.

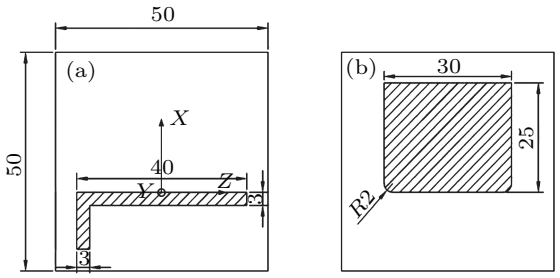


Fig. 1. Geometry of the DBD plasma actuator: (a) exposed electrode and (b) encapsulated electrode.

2.2. Experimental apparatus

A schematic diagram of the experiment is shown in Fig. 2. An AC power supply (CTP-2000K) is used for the discharge. The applied voltage and the discharge current are measured using a high voltage probe (Tektronix P6015A) and a current probe (Tektronix, TCP0030A). Traces of the discharge voltage and the current waveform are displayed and recorded by a digital oscilloscope (Tektronix, DPO4014). The discharge is performed at atmospheric pressure in static air. A digital camera (Nikon, D7000) is used to capture the plasma images. A digital microscopic system (KH-8700) is used to characterize the surface morphologies of ceramic dielectrics before and after discharge aging. The power consumption is calculated using the probe capacitor method. As shown in Fig. 2, a probe capacitor with a capacitance of 10 nF is placed between the encapsulated electrode and the ground. The discharge/charge is measured through the probe capacitor. Then, the power consumption can be obtained from the oscilloscope screen by plotting the transported charge on the Y axis and the applied voltage on the X axis. The following formula is used to calculate the discharge power:

$$P = \frac{1}{T}\int_0^T UI\,\mathrm{d}t = \frac{C_\mathrm{M}}{T}\int_0^T U\frac{U_{C_\mathrm{M}}}{\mathrm{d}t}\,\mathrm{d}t$$
$$= fC_\mathrm{M}\oint U\,\mathrm{d}U_{C_\mathrm{M}} = fC_\mathrm{M}S, \quad (1)$$

where T and f represent the cycle of the power supply and the working frequency, respectively. The parameter S denotes the area of the Lissajous figure. The discharge power P is proportional to S.

Surface temperature measurement is conducted using a thermal camera FLIR System (SC7000) in the spectral range of 7.7 μm–9.3 μm. New AlN actuator and Al_2O_3 actuator are prepared and the surfaces are coated with a layer of nonconductive black paint with a known thermal emissivity (ε) of

0.95. The camera records the infrared emission of the dielectric surface, which is a function of the actual temperature. It is placed 20 cm above the discharge.

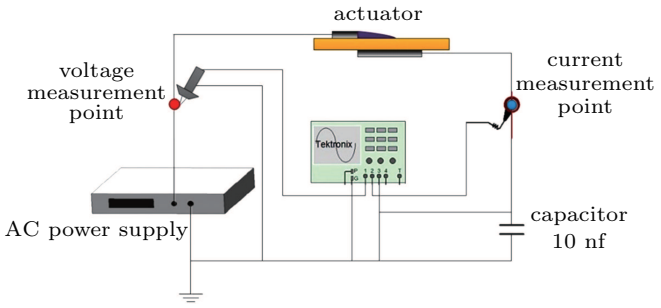


Fig. 2. (color online) Schematic diagram of the experiment.

A pressure probe made of glass tube (0.5-mm outer bore and 0.3-mm inner bore) is used to measure the induced gas flow. The actuators are mounted on a manual displacement system (Zolix PSA100-11-X) with an accuracy of ±0.1% that permits displacements along three directions. The pressure probe is placed at a distance of 0.05 mm from the dielectric wall. The pressure is measured using a micro differential pressure sensor (K0166), which permits ±10-Pa measurements with an accuracy of ±0.05%. An A/D converter (8 inputs, 10 kS/s, 12 bit) is used to sample the manometer output.

3. Results and analysis

3.1. Plasma images and thermal characteristics

The plasma images are captured using a camera (Nikon D7100), the applied voltage was modified from 6 kV to 15 kV, and the power supply frequency was set to be 11 kHz. As shown in Fig. 3, the discharge images of the two actuators appear to be relatively uniform along the exposed electrode length (spanwise direction) when the voltage is less than 11 kV. As the applied voltage continues to increase, for the Al_2O_3 actuator, the discharge regime evolves into more intense and longer filaments accompanied by an extended plasma, these filaments are concentrated at several points along the exposed electrode. However, distinct filaments cannot be clearly observed until the voltage is increased to 15 kV for the AlN actuator.

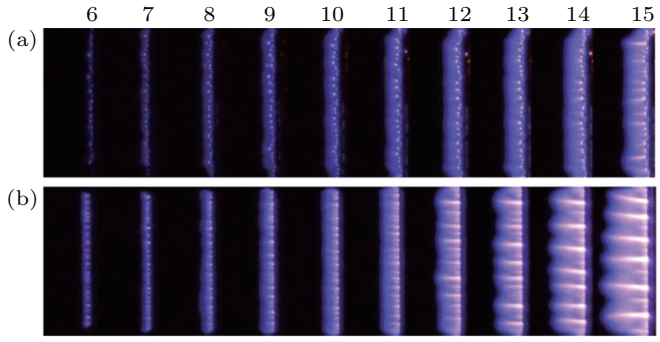


Fig. 3. (color online) Plasma generated by (a) AlN actuator and (b) Al_2O_3 actuator, applied voltage amplitude is listed above each image column in unit kV.

Since the rise in temperature near the edge of the exposed electrode is highest, it can be used as a method to characterize discharge uniformity of the actuator.[24,25] Thus, the surface temperature along the Z direction is further measured by a thermal infrared imager. The actuators are run for a duration of 120 s and then switch off for 30 s. The applied voltages are 8 kV, 10 kV, and 12 kV at a fixed frequency of 11 kHz. The room temperature in this experiment is 17 °C. Figure 4 shows the temperature distributions along the edge of the exposed electrode ($x = 0$ mm) at the end of a 120 s discharge run with different applied voltages. The peaks superimposed on the curves visually depict the temperature values of the discharge filaments. As can be seen, when the applied voltage is increased from 8 kV to 12 kV, the corresponding values of these peaks increase more sharply for the Al_2O_3 actuator, which indicates that its filaments are more intense. Besides, ΔT value, which means the temperature difference between the maximum and minimum along the edge of the exposed electrode, is further calculated to evaluate the temperature fluctuation. As illustrated in Fig. 4(b), ΔT values of the Al_2O_3 actuator at 8 kV, 10 kV, and 12 kV are 5.2 °C, 8.4 °C, and 31.5 °C, which are 1.93, 2.05, 3.25 times as large as those of the AlN actuator, respectively. Therefore, it can be concluded that the AlN actuator can produce a more uniform discharge than the Al_2O_3 actuator.

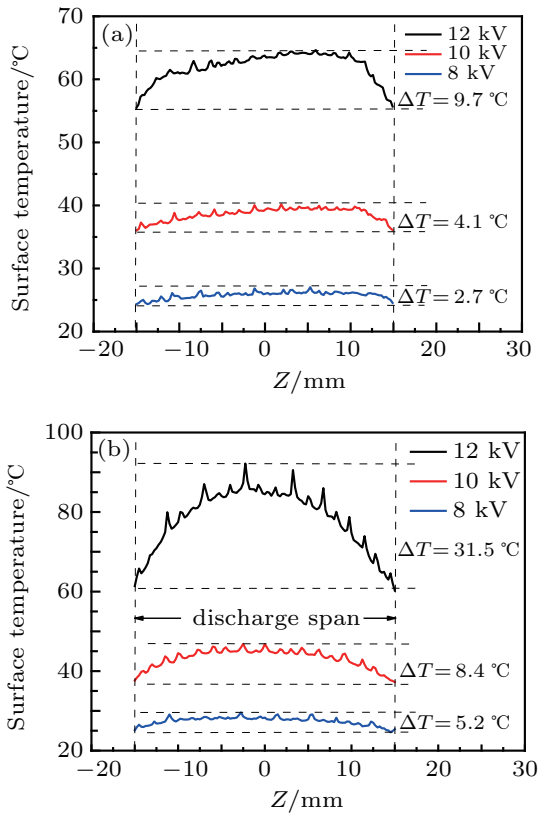


Fig. 4. (color online) Spanwise temperature distributions of (a) the AlN actuator and (b) the Al_2O_3 actuator.

3.2. Electrical properties

Figure 5 shows typical curves of DBD discharge current and applied voltage versus time when the voltage is 12 kV and the frequency is 11 kHz. In the case of the AlN actuator, during the positive half of the cycle, many of the current peaks reach values between 60 mA and 80 mA (Fig. 5(a)). The current peaks of the Al_2O_3 actuator shown in Fig. 5(b) are higher than those of the AlN actuator, attaining 100 mA to 150 mA. It can be speculated that the higher current pulse peaks may result from more intense filamentary discharge, which is consistent with the results of plasma morphologies shown in Fig. 3(b) and surface temperature shown in Fig. 4(b). In general, the appearance of these current peaks is due to streamer propagation where each pulse corresponds to one microdischarge that distributes across the electrodes. A microdischarge is a small channel of charge that lasts a few nanoseconds[26] and terminates on the dielectric surface. Charges are aggregated on the dielectric surface, which reduces the electric field strength across the discharge gap, thus leading to the termination of the discharge.

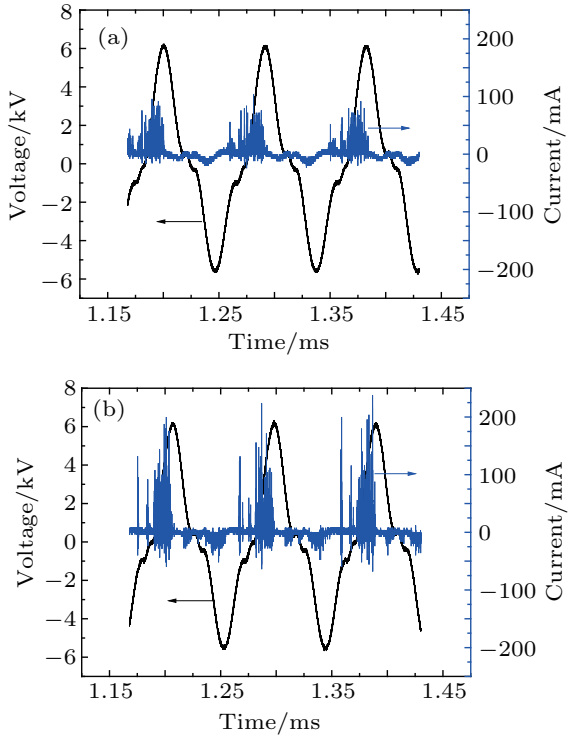


Fig. 5. (color online) Traces of discharge current and applied voltage of (a) AlN actuator and (b) Al_2O_3 actuator.

Figure 6(a) shows the power consumption per unit length as a function of applied voltage. For the two actuators, the active power per centimeter varies as $P_{el} \propto (V_{pp})^n$, which is similar to the law found in previous studies.[7] The active power P_{el} (W/cm) can be estimated by the empirical law[27]

$$P_{el} = C_{act} f_{ac} L_{act} (V_{pp})^n. \quad (2)$$

Here, C_{act} is a coefficient that depends on the geometric arrangement of the actuator, f_{ac} is the power frequency, L_{act} is the characteristic spanwise length of the exposed electrode, and V_{pp} is the high voltage amplitude. The coefficient C_{act} and the exponent n are obtained by fitting (least-squares method) the experimental data to the Pons expression.

The values of L_{act}, C_{act}, and n are used to estimate the active power as summarized in Table 1. It can be seen that the exponent n of the AlN actuator is within the range value reported in previous literature[28,29] while that of the Al_2O_3 actuator ($n = 5.30$) is out of the range.

Table 1. Parameters of the empirical power law (2).

Dielectrics	L_{act}/m	C_{act} /W·m^{-1}·Hz^{-1}·V^{-n}	n	R^2
Al_2O_3	0.03	2.12×10^{-8}	5.30	0.99
AlN	0.03	2.91×10^{-6}	3.19	0.99

The plots of power per unit area versus applied voltage are given in Fig. 6(b). When the applied voltage is lower than 9 kV, the active power per square centimeter of the Al_2O_3 actuator is lower than that of the AlN actuator. As the applied voltage is higher than 9 kV, the increase of the power with the Al_2O_3 actuator becomes more obvious. This result is mainly caused by the intense filamentary discharge of the Al_2O_3 actuator. Inside these filaments, charge transfer increases locally, which causes the streaks to become brighter and hotter. Therefore, the average energy density increases more significantly for the Al_2O_3 actuator than for the AlN actuator.

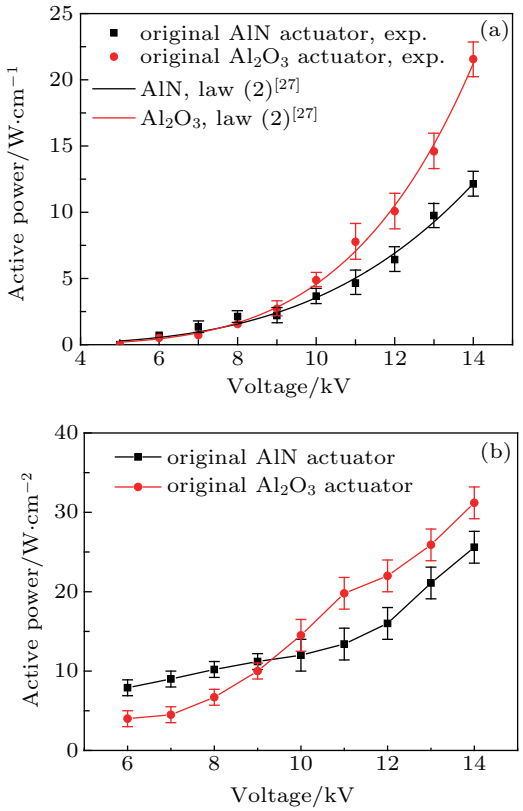


Fig. 6. (color online) Comparison of plots of active power (a) per unit length and (b) per unit area versus applied voltage between the AlN actuator and the Al_2O_3 actuator.

3.3. Surface morphologies and corresponding plasma images

The surface morphologies and corresponding plasma images of the actuators obtained from aging experiments are shown in Fig. 7. All the experiments below are conducted with the same power supply parameters: 12-kV applied voltage and 11-kHz power frequency, and 30-min aging cycle. As shown in Fig. 7(a), for the AlN actuator, the plasma discharge region expands with the discharge time. After 60-min discharge aging, the black discharge stripes remain on the surface of the AlN ceramic. As the operation time goes on, these stripes propagate along both the spanwise direction and streamwise direction. For the Al_2O_3 actuator, there is no significant change in the discharge area as shown in Fig. 7(b). From the discharge region it can be seen that several intense filaments are present at all times. Furthermore, after 150-min operation, two bright burning points appear on the edge of the exposed electrode.

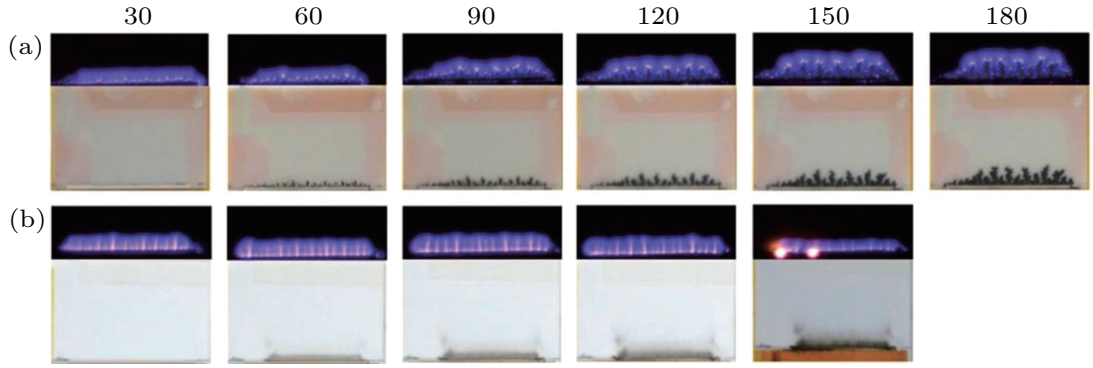


Fig. 7. (color online) Surface morphologies and corresponding plasma images of (a) the AlN actuator and (b) the Al_2O_3 actuator. Operation time is listed above each image column in unit min.

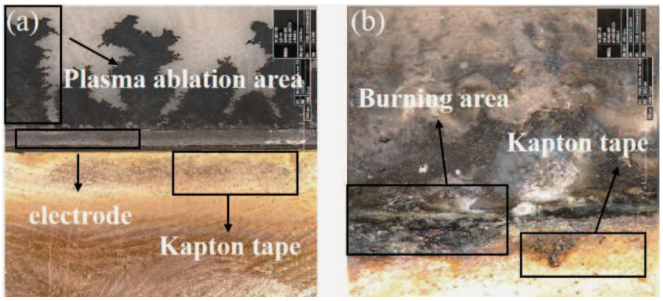


Fig. 8. (color online) Enlarged surface morphologies around the exposed electrode taken from the surfaces of (a) AlN actuator and (b) Al_2O_3 actuator.

Figure 8 shows the enlarged surface morphologies of the AlN actuator and the Al_2O_3 actuator after 150-min operation. The exposed electrodes of the aged actuators are both oxidized in comparison with the original actuators. The oxidation of the Al_2O_3 actuator appears to be more serious, which can be explained by the fact that a small part of Kapton tape on the edge of its exposed electrode is burned. The result indicates that the continuous, intense discharge filaments can cause the electrode to be unstable and lead to earlier failure of the actuator prior to the breakdown of the dielectric as shown in Fig. 8(b). Besides, it can also be observed that many burred areas ablated by plasma are distributed around the remaining discharge stripes of the AlN actuator, which are consistent with the bright discharge points shown in Fig. 7(a).

3.4. Variation of power consumption after discharge aging

To determine the effects of discharge duration on consumed power, the actuators aged for various times are prepared and their consumed powers are calculated through the Lissajous figures.

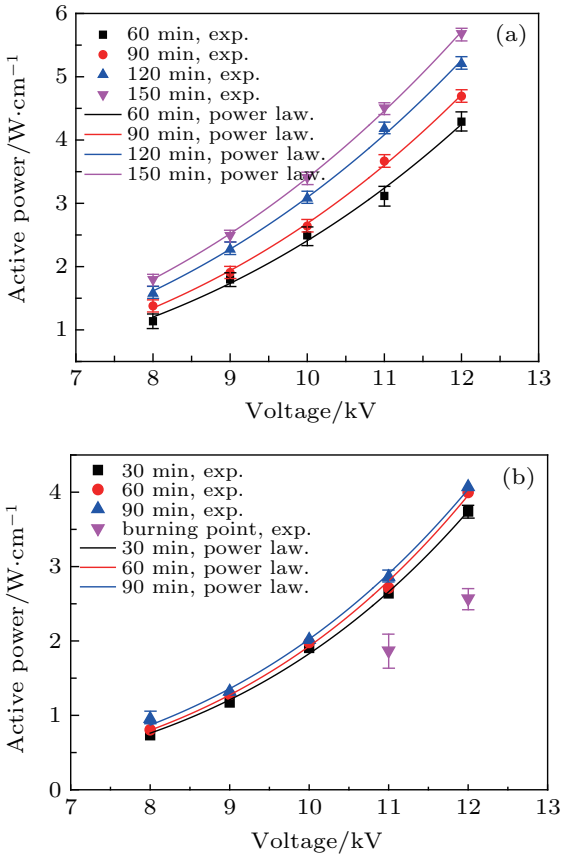


Fig. 9. (color online) Variations of active power with applied voltage for (a) AlN actuator and (b) Al_2O_3 actuator for different discharge times; symbols are related to the experimental data sets; the lines denote the power consumptions obtained from Eq. (2).

As shown in Fig. 9, for the AlN actuators, discharge times are 60 min, 90 min, 120 min, and 150 min, respectively. For the Al_2O_3 actuator, the discharge times are 30 min, 60 min, and 90 min, respectively. It can be seen that the power consumption of the aged actuator continues to maintain a power relationship with the increase of applied voltage as described by Pons *et al.*[7]

As shown in Table 2, when the discharge time is increased from 60 min to 150 min, the power law value for the AlN actuator decreases from 3.11 to 2.84, which indicates that the effect of applied voltage on power is reduced after a long duration of discharge. The Al_2O_3 actuator also exhibits a similar trend. Moreover, the previously described electrode oxidation has a significant effect on power consumption. The pink data points shown in Fig. 9(b) reveal that the power consumptions decrease by 73.1% and 74.4% compared with the 30-min operation for the Al_2O_3 actuator.

Table 2. Parameters of the empirical power law (Eq. (2)) for aged ceramic dielectric.

Dielectrics	Operation/min	C_{act} /W·m^{-1}·Hz^{-1}·V^{-n}	n	R^2
AlN	60	2.08×10^{-6}	3.11	0.99
	90	1.11×10^{-6}	3.09	0.99
	120	2.14×10^{-6}	2.91	0.99
	150	1.37×10^{-6}	2.84	0.99
Al_2O_3	30	6.52×10^{-7}	3.93	0.99
	60	6.70×10^{-7}	3.92	0.99
	90	1.00×10^{-6}	3.78	0.99

3.5. Induced velocity characteristics

The effects of dielectric aging on the induced velocities of the actuators are investigated through the pressure probe measurements. The values of y distance (vertical height from the upper surface of the actuator dielectric to the lower side of the Pitot tube) are set to be 0.2 mm, 0.5 mm, and 0.8 mm for various conditions. For each measurement, the Pitot tube is placed at a fixed vertical height and moved from $x = 0$ mm to $x = 22.5$ mm, at a speed of 0.5 mm/s. Each measurement is repeated 3 times. The time-averaged horizontal component of the ionic wind velocity is obtained from the Bernoulli equation:

$$V = \sqrt{2 \times P/\rho}, \tag{3}$$

where P is the dynamic pressure, which is equal to the total pressure minus the static pressure, and ρ (≈ 1.29 kg/m^3) is the gas density under the standard condition.

The evolutions of velocity for the two actuators are shown in Fig. 10. The first series of measurements of the velocity profiles before dielectric aging is shown in Fig. 10(a) for the Al_2O_3 actuator and in Fig. 10(d) for the AlN actuator. For both two actuators, the velocities increase from the edge of the exposed electrode, attain a maximum and then decrease, which can be explained by the viscosity effects on the surface of the dielectric. In addition, it can be seen that at the $y = 0.2$ mm, the velocities of the two actuators reach their maximum values at almost the same x position. The maximum velocity of the AlN actuator is higher than that of the Al_2O_3 actuator (4.2 m/s versus 3.0 m/s). This is due to the more homogenous discharge of the AlN actuator. After y distance is increased from 0.2 mm to 0.5 mm, the induced velocity of the AlN actuator decreases faster than that of the Al_2O_3 actuator with the increase of the x location. For instance, at $x = 22.5$ mm and $y = 0.2$ mm, 0.5 mm, and 0.8 mm, the velocities of the AlN actuator are 36%, 39%, and 31% lower than that of the Al_2O_3 actuator, respectively. Therefore, it can be concluded that a greater induced velocity occurs in the AlN actuator while the longer ionic wind diffusion is induced with the Al_2O_3 actuator.

The second series of measurements after 60 min of dielectric aging is shown in Figs. 10(b) and 10(e). It can be seen that the maximum velocities of the AlN actuator at three y positions (0.2 mm, 0.5 mm, and 0.8 mm) are all greater than those of the Al_2O_3 actuator. Besides, compared with the maximum velocities of the un-aged actuators, the maximum velocities of the Al_2O_3 actuator at positions $y = 0.2$ mm, 0.5 mm, and 0.8 mm decrease from 3.0 m/s, 2.2 m/s, and 1.72 m/s to 2.56 m/s, 2.0 m/s, and 1.64 m/s, respectively, while maximum velocities of the AlN actuator decrease from 4.2 m/s, 3.58 m/s, and 3.09 m/s to 3.33 m/s, 2.85 m/s, and 2 m/s, respectively. Also, no velocity value is found after the x position has exceeded 14 mm for the AlN actuator at $y = 0.2$ mm.

The third series of measurements after 120 min of dielectric aging is shown in Figs. 10(c) and 10(f). For both actuators, the maximum velocities continue to decrease at different y positions. Compared with the maximum velocities of the actuators without dielectric aging, at $y = 0.2$ mm, 0.5 mm, and 0.8 mm the maximum velocities of the Al_2O_3 actuator decrease by 25%, 10.5%, and 6.4 m/s, respectively. While the maximum velocities of the AlN actuator decrease by 27.8%, 39.6%, and 43.7%, respectively. Although the maximum induced velocities of the AlN actuator after 120 min of discharge are higher than those of the Al_2O_3 actuator at all three y positions, it seems that dielectric aging has a greater effect on the induced velocity of the AlN ceramic.

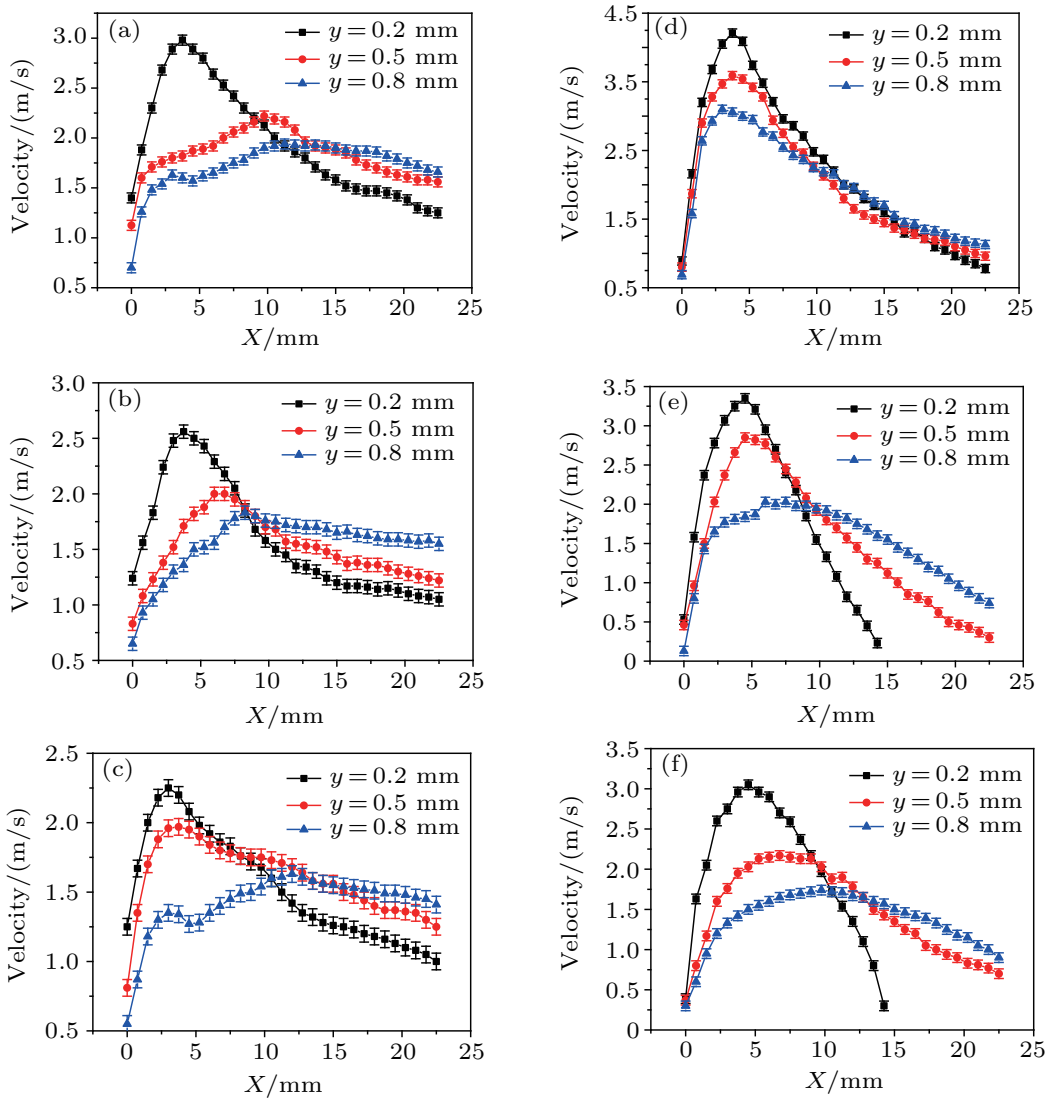


Fig. 10. (color online) Ionic wind velocities along the X direction of the Al_2O_3 actuator at (a) 1 min, (b) 60 min, and (c) 120 min and the AlN actuator at (d) 1 min, (e) 60 min, and (f) 120 min.

4. Conclusions

The electrical properties, material characteristics and induced velocities of the DBD plasma actuators with AlN and Al_2O_3 ceramic dielectrics are experimentally investigated. The main conclusions are as follows.

For the original actuators, either active power per unit length or per unit area, consumed by the Al_2O_3 actuator is higher than that of the AlN actuator when the applied voltage is greater than 9 kV. The plasma images reveal that long and intense discharge filaments occur in the Al_2O_3 actuator, but the discharge in the AlN actuator appears more uniformly. This uniformity is further evidenced by surface temperature measurement and current pulse behavior analysis.

For the aged actuators, the two ceramics exhibit different material characteristics. Severe electrode oxidation of the Al_2O_3 actuator, resulting from intense filaments causes its earlier failure. While for the AlN actuator, the surface is ablated and the traces extend along both the spanwise and streamwise directions as the operation time increases.

The maximum induced velocities of the AlN actuator along the X-direction are higher than those of the Al_2O_3 actuator at all three y positions (0.2, 0.5, 0.8 mm) before and after dielectric aging. However, long plasma process affects the induced velocities of two actuators. After 120min discharge operation, the maximum velocities of the aged AlN actuator and the Al_2O_3 actuator decrease by 27.8% and 25%, respectively.

References

[1] Wu Y, Li Y H, Jia M, Liang H and Song H M 2012 *Chin. Phys. B* **21** 045202
[2] Zhao G Y, Li Y H, Liang H, Hua W Z and Han M H 2015 *Acta Phys. Sin.* **64** 015101 (in Chinese)
[3] Moreau E 2007 *J. Phys. D: Appl. Phys.* **40** 605
[4] Corke T C, Post M L and Orlov D M 2009 *Exp. Fluids* **46** 1
[5] Benard N, Moreau E 2014 *Exp. Fluids* **55** 1846
[6] Forte M, Jolibois J, Pons J, Moreau E, Touchard G and Cazalens M 2007 *Exp. Fluids* **43** 917

[7] Pons J, Moreau E and Touchard G 2005 *J. Phys. D: Appl. Phys.* **38** 3635
[8] Dong B, Bauchire J M, Pouvesle J M, Magnier P and Hong D 2008 *J. Phys. D: Appl. Phys.* **41** 155201
[9] Pouryoussefi S G and Mirzaei M 2015 *Plasma Sci. Technol.* **17** 415
[10] Thomas F, Corke T, Iqbal M, Kozlov A and Schatzman D 2009 *AIAA J.* **47** 2169
[11] Abe T, Takizawa Y, Sato S and Kimura N 2007 45*th AIAA Aerospace Sciences Meeting*, January 8–11, 2007, Reno, Nevada, p. 187
[12] Durscher R, Stanfield S and Roy S 2012 *Appl. Phys. Lett.* **101** 252902
[13] Park H W, Cho I J, Choi S and Park D W 2014 *IEEE Trans. Plasma Sci.* **42** 2364
[14] Durscher R and Roy S 2012 *J. Phys. D: Appl. Phys.* **45** 012001
[15] Michael J J and David B G 2014 *Appl. Phys. Lett.* **105** 264102
[16] Fine N E and Brickner S J 2010 *AIAA J.* **48** 2979
[17] Starikovskiy A and Miles R 2013 *51st AIAA Aerospace Sciences Meeting*, January 7–10, 2013, Dallas, Texas, USA, p. 754
[18] Opaits D, Zaidi S, Shneider M and Miles R 2009 39*th AIAA Fluid Dynamics Conference*, June 22–25, 2009, San Antonio, Texas, USA, p. 4189
[19] Hanson R E, Kimelman J, Houser N M and Lavoie P 2014 *J. Appl. Phys.* **115** 043301
[20] Hanson R E, Kimelman J, Houser N M and Lavoie P 2013 51*st AIAA Aerospace Sciences Meeting*, Grapvine, TX, p. 397
[21] Ndong A C, Zouzou N, Benard N and Moreau E 2013 *IEEE Trans. Dielec. Electr. Insul.* **20** 1554
[22] Luo Y, Wu G N, Liu J W, Peng J, Gao G Q, Zhu G Y, Wang P and Cao K J 2014 *Chin. Phys. B* **23** 027703
[23] Pons J, Oukacine L, Moreau E and Tatibouët J M 2008 *IEEE Trans. Plasma Sci.* **36** 1342
[24] Biganzoli I, Barni R, Gurioli A, Pertile R and Riccardi C 2014 *J. Phys. C: Conference Series* **550** 012038
[25] Tirumala R, Benard N, Moreau E, Fenot M, Lalizel G and Dorignac E 2014 *J. Phys. D: Appl. Phys.* **47** 255203
[26] Laurentie J C, Jolibois J and Eric Moreau 2009 *J. Electrost.* **67** 93
[27] R Joussot, A Leroy, R Weber, H Rabat, S Loyer and D Hong 2013 *J. Phys. D: Appl. Phys.* **46** 125204
[28] Kriegseis J, Eoller B M, Grundmann S and Tropea C 2011 *J. Electrost.* **69** 302
[29] Murphy J P, Kriegseis J and Lavoie P 2013 *J. Appl. Phys.* **113** 243301